Acta Cryst. (1995). A**51**, 801–809

Structure Determination of a Rhombohedral Al–Ge Phase by CBED and X-ray Powder Diffraction

BY R. VINCENT AND D. R. EXELBY

H. H. Wills Physics Laboratory, University of Bristol, Tyndall Avenue, Bristol BS8 1TL, England

(*Received* 26 *December* 1993; *accepted* 15 *May* 1995)

Abstract

A new approach to the problem of crystal structure determination by electron diffraction is described based upon the intensities of higher-order Laue-zone (HOLZ) reflections in convergent-beam electron diffraction (CBED) patterns. Along a major zone axis, a subset of symmetry-related atoms may project into separate string potentials associated with localized Bloch states. In a quasi-kinematic limit, the amplitudes of HOLZ excess lines diffracted from the Bloch states are proportional to the partial structure factors for these atoms. If a structure is unknown, the Bloch states cannot be calculated but it is shown that the conditional Patterson transform of the HOLZ intensities around suitable axes may include narrow correlation peaks that identify interatomic vectors. This approach was tested by analysis of a metastable Al–Ge phase with space group $R\bar{3}c$. A transform of HOLZ intensities measured around the c axis showed peaks displaced by only 0.21 Å from the screw axes, consistent with Ge atoms in the 18(e) positions. Although Al atoms were not visible in the Patterson maps, the crystal structure with nominal composition Al_6Ge_5 was identified as isostructural with the Zn_4Sb_3 phase by comparison of observed and calculated X-ray powder intensities.

1. Introduction

The general problem of *ab initio* structure determination by electron diffraction for an inorganic crystalline phase remains only partially solved despite recent advances in instrumentation and image processing. A direct approach based on interpretation of lattice images projected along axes where the atom strings are well separated is necessarily limited by the point resolution of the electron microscope, although new techniques such as side-band holography (Lichte, 1992), phase extension by direct methods adapted from X-ray crystallography (Dong *et al.*, 1992) and processing of through-focal sequences (Coene, Janssen, Op de Beeck & Van Dyck, 1992) are reducing the resolution limit towards 1 Å. Nevertheless, a resolution of 1 Å is insufficient to infer the three-dimensional structure of even a moderately complex crystal, quite apart from the problem of dealing with dynamical coupling between beams diffracted around a major zone axis. By analogy with X-ray crystallography, it is essential to use the medium- and high-order reflections to improve atomic resolution within the unit cell and provide a reliable measure of bond lengths and coordination chemistry. For thin organic crystals and also layered or textured inorganic crystals containing principally light elements, the limitations produced by dynamical coupling between reflections are less severe, and considerable progress has been made by application of standard X-ray methods for structure determination, as reviewed by Cowley (1965) and more recently by Vainshtein, Zvyagin & Avilov (1992). In an extension of this research, Dorset (1991, 1992) has shown that direct methods for phasing reflections may be successfully applied in the limit of kinematic electron diffraction around zone axes, where accuracy is limited mostly by curvature of the Ewald sphere combined with sparse sampling of the reciprocal lattice.

From this viewpoint, an approach based principally upon convergent-beam electron diffraction (CBED), directed towards solution of the inverse problem of inferring structure factors from dynamical intensities, represents a more efficient use of the available information. For example, comparison of the experimental and calculated intensities for the lowest-order reflections in a known structure is used to measure the amplitudes and phases of structure factors with high accuracy and thereby reconstruct the bonding charge distribution (Spence & Zuo, 1992; Bird & Saunders, 1992). However, the information needed to solve an unknown structure lies at the opposite extreme, in that we require the efficient collection of a large set of intensities for higher-order reflections measured with moderate accuracy and subject to limited dynamical perturbations so that methods developed for analysis of X-ray data remain applicable. A further condition is that data acquisition should be compatible with the practical problems of recording CBED patterns from sub-micrometre crystals in a specimen that may contain a complex mixture of phases processed under non-equilibrium conditions.

In a previous publication (Vincent & Bird, 1986), a new CBED technique for measurement of kinematic intensities was described, where a beam with a large convergence angle was focused onto the specimen

parallel to a zone axis. The discs of the diffracted orders overlapped but remained separable for higher-order Laue-zone (HOLZ) reflections because electrons were diffracted only into narrow excess lines mapping the Bragg conditions. Being higher-order reflections in weak systematic rows and subjected only to local perturbations by non-systematic interactions, the diffracted intensities remained approximately kinematic in thin crystals and were suitable for structure analysis. The technique was applied to a tetragonal Al–Ge phase grown by recrystallization of vapour-quenched films (Vincent & Exelby, 1993), where conditional Patterson transforms of the HOLZ intensity data around the c axis showed clear peaks associated with inter-atomic vectors.

However, severe practical problems were encountered with the acquisition and indexing of excess lines due to the low visibility of HOLZ lines around a major axis relative to the diffuse background from multiple overlapping discs. In addition, spherical aberration increased the focused probe size to 0.2 μm, implying that the crystal thickness exceeded the kinematic limit for some strong reflections. It was found necessary to measure intensities by combining data from HOLZ reflections excited around several minor axes close to the [001] direction. The problems of data collection were compounded for a crystal with a larger unit cell, and it was decided to rely upon standard CBED patterns recorded with a small probe size (~10 nm) and non-overlapping discs to investigate another metastable Al–Ge phase with a rhombohedral cell. The reduced angular field within discs both restricts the number of reflections excited within a single pattern around minor axes and increases the probability of not recognizing severe local variations of intensity associated with non-systematic interactions. However, diffraction around major axes often conforms to a simpler model related to the kinematic approximation, where electrons are scattered into HOLZ reflections, not from the incident plane wave but from Bloch states channelled along string potentials. The utility of this model for structure determination is discussed below.

2. HOLZ diffraction

The basis of this new approach to structure determination was an extension of a previously established method for refinement of atomic parameters by analysis of HOLZ intensities (Vincent, Bird & Steeds, 1984; Bird, 1989; Vincent & Withers, 1987). In the kinematic limit, the effective potential controlling the amplitudes of HOLZ reflections in the nth layer of the reciprocal lattice perpendicular to the c axis is given by the conditional projected potential $U^n(\mathbf{R})$, defined as

$$U^n(\mathbf{R}) = \int_0^1 U(\mathbf{r}) \exp(-2\pi i n z)\, \mathrm{d}z, \qquad (1)$$

where $U(\mathbf{r})$ is the crystal potential in standard notation, $\mathbf{R}$ is a position vector within the projected cell and z is a fractional coordinate. Substitution of the Fourier expansion of $U(\mathbf{r})$ gives the equivalent form of (1):

$$U^n(\mathbf{R}) = \sum_{\mathbf{G}_n} U_{\mathbf{G}_n} \exp(2\pi i \mathbf{G}_n \cdot \mathbf{R}), \qquad (2)$$

where $\mathbf{G}_n$ is a vector in the nth layer of the reciprocal lattice and $U^n(\mathbf{R})$ is a Fourier sum over $U_{\mathbf{g}}$ restricted to the nth layer. For $n = 0$, (1) and (2) reduce to the usual definitions of $U^0(\mathbf{R})$, the projected potential. Generally, the conditional potentials are simply a convenient formulation in real space of the information implicit in the structure factors, where a phase factor is attached to the atomic string potentials projected along the c axis. For example, identical atoms with the same $\mathbf{R}$ coordinate separated by $z = 1/2$ are absent from $U^n(\mathbf{R})$ for n odd.

However, HOLZ reflections diffracted around a major zone axis often show distinct excess lines slightly displaced from the Bragg condition, corresponding to diffraction out of excited Bloch states for the projected potential. The complete electron wave function is represented by a sum over the relatively few Bloch states with significant excitation. The most tightly bound branches that diffract into HOLZ excess lines inside the Bragg condition correspond to Bloch states localized on atom strings in the projected potential, where the effective conditional potential is modified to $U^n(\mathbf{R})$ multiplied by the Bloch amplitude $\tau^{(j)}(\mathbf{R})$ for branch j of the dispersion surface. The multiplication of a sharply localized string potential by the slowly varying function $\tau(\mathbf{R})$ implies that the shape and depth of atom strings is modified but the positions of projected atoms are not affected to a good approximation. For simple structures, the most tightly bound branch of the dispersion surface is likely to be a 1s state localized on a single string per cell in a high-symmetry position. It follows that the corresponding partial structure factors controlling diffraction into the inner excess line are invariants for all reflections within a HOLZ ring and the intensities show no azimuthal variation. For larger projected cells that contain several sets of symmetry-related strings, the localized states are more complex but dynamical calculations show a predictable pattern, where a cluster of molecular Bloch states is excited, being symmetric and antisymmetric combinations of 'atomic' 1s states localized on individual strings. Provided that the string potentials are well separated, the splitting between branches of the dispersion surface for the molecular states remains small, and the branch cluster can be treated as a single composite Bloch state localized on all of the symmetry-related strings, at least for crystal thicknesses much less than interbranch extinction distance within the cluster (Vincent *et al.*, 1984). When multiplied by $U^n(\mathbf{R})$, the effect is to isolate a subset of symmetry-related atom strings within the conditional potential and it follows that the amplitudes of the related HOLZ excess

lines remain proportional to the corresponding partial structure factors in a quasi-kinematic limit where the crystal thickness is much less than HOLZ extinction distances. Provided that the localization and excitation of Bloch states are known from dynamical calculations for the approximate crystal structure, HOLZ intensities may be used to refine atomic parameters and calculate bond lengths with a precision approaching measurements based on X-ray data.

A further assumption implicit in this argument is that dynamical coupling between HOLZ reflections does not perturb intensities sufficiently that the quasi-kinematic approximation described above becomes invalid. In the absence of a detailed comparison with dynamical calculations for a given zone axis, any argument to this effect must be based upon practical experience. Certainly, some HOLZ excess lines show azimuthal variations of intensity, attributed to coupling *via* strong zero-layer reflections. These reflections may be omitted from the structure refinement but a more practical option that minimizes the effect of individual perturbations is to measure the averaged intensities for a large number of HOLZ reflections. Provided that the HOLZ reflections are high multiples of the reciprocal basis vectors, even small atomic displacements produce large changes in the associated structure factors. The reliability factor, R, for the refined structure is defined as

$$R = \sum |A_o - A_c| / \sum A_o, \tag{3}$$

where A_o and A_c are the observed and calculated amplitudes, respectively. By X-ray standards, typical values of R for structures refined from HOLZ intensities are quite large (~ 0.3) owing to dynamical perturbations, but still correspond to high accuracy in the atomic parameters.

In practice, the excitation and dispersion of the localized Bloch states considered here remain almost constant within the first Brillouin zone around a major axis, providing a convenient method for measuring a large number of HOLZ intensities because the intensity of a localized excess line becomes almost independent of position within a HOLZ disc. If successive CBED patterns are acquired at accelerating voltages separated by small intervals (10–20 kV), excess lines within any reflection remain visible in two or more patterns, and are suitable for cross-calibration or overall scaling of intensities. In principle, the localization of Bloch states changes between patterns recorded at different voltages because $U(\mathbf{r})$ is proportional to γ, the relativistic mass ratio. However, γ increases by only 25% between 100 and 300 kV, and calculations have shown that changes in the shape of the modified string potentials defined by $\tau(\mathbf{R})U^n(\mathbf{R})$ have little effect on the relative magnitudes of quasi-kinematic structure factors around a ring of HOLZ reflections. Any variations of thickness and/or localization between patterns recorded at different voltages are absorbed into the scaling factors mentioned above.

Even if a structure is completely unknown, it is likely that the HOLZ intensities around some major axes contain useful information about interatomic vectors that may be extracted from conditional Patterson transforms with no previous knowledge of the Bloch states. Patterson transforms are not widely used in modern X-ray crystallography, partly due to the use of direct methods for phasing reflections, and also because N atoms within the cell generate up to $N^2 - N$ independent peaks representing interatomic vectors, leading to problems of interpretation due to peak overlap compounded by broadening of peaks due to convolution. The Patterson transform is defined here as

$$P(\mathbf{r}) = (1/V)\int U(\mathbf{r}')U(\mathbf{r}+\mathbf{r}')\,\mathrm{d}\mathbf{r}', \tag{4}$$

where V is the cell volume. Definitions of the conditional projections apply equally to the Patterson function, where

$$P^n(\mathbf{R}) = \int_0^1 P(\mathbf{r})\exp(-2\pi i n z)\,\mathrm{d}z \tag{5}$$

and

$$P^n(\mathbf{R}) = \sum_{\mathbf{G}_n} U_{\mathbf{G}_n}^2 \exp(2\pi i \mathbf{G}_n \cdot \mathbf{R}). \tag{6}$$

If the $U_{\mathbf{G}_n}$ components in (6) represent partial structure factors from a limited subset of atoms in the cell and the summation is restricted to the intensities of HOLZ reflections, interpretation is simplified, both by the reduction of the effective value for N and also because the absence of low-order reflections sharpens peaks and reduces overlaps. The observation of a clear set of peaks with high visibility relative to the background ripples due to series termination constitutes a reliable, accurate and independent guide to the structure. Conversely, the absence of interpretable peaks in a transform is likely to imply that the structure does not project into clearly separated string potentials along a particular axis and that the corresponding Bloch states have unpredictable localization, excitation and eigenvalues.

In summary, most zone axes are likely to be unsuitable for calculation of HOLZ Patterson transforms. Properties of an ideal axis are listed below:

(1) We require densely populated and well separated reciprocal-lattice planes normal to the zone axis to increase both the separation of atom strings and the order of HOLZ reflections.

(2) Axes parallel to mirror planes and/or rotation axes in the space group are preferred because geometrical constraints on the minimum separation of atoms are likely to reduce overlap of atom strings.

(3) HOLZ reflections should show a distinct inner excess line with large intensity differences between equivalent excess lines in adjacent discs.

(4) Diffraction from localized Bloch states is confirmed by rapid absorption of intensity with increasing thickness, combined with no evidence of dispersion within the first Brillouin zone, and with clear separation from other excess lines diffracted at larger angles from weakly localized or channelling states.

(5) Absence of any visible fine structure in excess lines with increasing thickness, consistent with diffraction from a set of weakly split molecular states localized on separate strings.

As a practical test, the unknown structure of a rhombohedral Al–Ge phase was examined by use of HOLZ Patterson transforms. A summary of this research has been previously published (Vincent & Exelby, 1991).

Table 1. *Comparison of structural parameters for the R phase of* Al_6Ge_5 *and* Zn_4Sb_3 *(space group* $R\bar{3}c$*)*

	Al_6Ge_5	Zn_4Sb_3
Lattice parameters (Å)	$a = 11.45$	$a = 12.223$
	$c = 11.67$	$c = 12.428$
	$c/a = 1.019$	$c/a = 1.016$
Atomic parameters	Al in 36(f)	Zn in 36(f)
		$x = 0.079$
		$y = 0.244$
		$z = 0.404$
	Ge1 in 12(c)	Sb in 12(c)
	$x = y = 0$	$x = y = 0$
		$z = 0.137$
	Ge2 in 18(e)	$Zn_{0.11}Sb_{0.89}$ in 18(e)
	$x = 0.352$	$x = 0.355$
	$y = 0$	$y = 0$
	$z = 0.25$	$z = 0.25$
Reference	Kaufman & Fraser (1985) and present work	Mayer *et al.* (1978)

3. Al–Ge CBED patterns

Rapidly quenched alloy ribbons with average composition $Al_{0.64}Ge_{0.36}$ were grown by melt-spinning, where the liquid alloy was ejected by Ar gas onto a Cu wheel rotating with a surface velocity of $22\,m\,s^{-1}$. Fragments were electropolished (10% perchloric acid in ethanol), followed by a brief etch with Ar ions to clean the surfaces, and were examined in a Philips EM430 electron microscope at voltages between 100 and 250 kV. Specimens were cooled to 100 K to reduce thermal diffuse scattering. The major component in the ribbons was a rhombohedral phase with an average grain size of 0.5 μm, combined with a monoclinic Al–Ge phase and some α-Al grains. CBED patterns acquired with a probe size of 10 nm parallel to the major axes of the rhombohedral phase (referred to below as the R phase) confirmed the space group as $R\bar{3}c$; the relevant CBED patterns are illustrated in Figs. 6 and 7 of Kaufman & Fraser (1985). Lattice parameters listed in Table 1 for the hexagonal non-primitive cell were measured both from electron spot patterns and also from X-ray powder patterns (see below). The values for c and a in Table 1 agree with the R cell parameters listed by Kaufman & Fraser (1985) to within 0.1% when converted from the rhombohedral P cell to the hexagonal axes used here. Likewise, the R phase composition measured from calibrated energy-dispersive X-ray (EDX) spectra was equiatomic AlGe within error limits of a few percent, in agreement with Kaufman & Fraser (1985).

The estimated number of atoms in the primitive cell varied between 22 and 26, depending on assumptions about the coordination and associated atomic volumes, implying that most atoms were likely to occupy sites within the cell with low site symmetry. As an initial approach to recognize regions of scattering associated with clusters of Al or Ge atoms projected along the c axis, a set of strong zero-layer reflections with indices of type $hki0$ ($h - k = 0 \bmod 3$) were selected. Suitable reflections within the $11\bar{2}0$ and $30\bar{3}0$ systematic rows were selected from large-angle CBED patterns as described by Ma, Romming, Lebech, Gjønnes & Taftø (1992), where it was evident that the excess lines mapping the Bragg conditions for $12,0,\bar{1}\bar{2},0$ and $33\bar{6}0$ reflections were more intense than their neighbours within the rows. Two other reflections subject to less perturbation by systematic effects were selected by indexing Kikuchi bands showing strong contrast. The four reflections, equivalent to $3\bar{6}$ for $6mm$ projection symmetry are plotted in Fig. 1(a), and each was assigned equal intensity, in recognition of the qualitative selection process and inevitable dynamical effects.

The reflections in Fig. 1(a) were all linked by closed vector loops, and it followed by application of direct methods that the origin-independent phase sum of the structure factors around any loop was likely to be zero. For the conventional choice of origin on a $\bar{3}$ inversion centre in $R\bar{3}c$ with $6mm$ phase symmetry for $hki0$ reflections and using X-ray conventions for the sign of structure factors, the only consistent solution was to assign zero phase to all indexed reflections. The inverse Fourier transform is shown in Fig. 1(b) for a symmetry-reduced sector within the projected cell, where scattering centres are located on both the $\bar{3}$ axes and the $3_{1,2}$ screw axes. The resolution of Fig. 1(b) was difficult to assess due to the omission of all weak reflections, but the planar spacings of components in the transform varied between 1.95 and 0.8 Å.

It was probable that tightly bound Bloch states occupied the $\bar{3}$ and $3_{1,2}$ axes in Fig. 3(b), and consequently the fine structure of [0001] first-order Laue-zone (FOLZ) reflections was examined for evidence of diffraction from subsets of atom strings located close to these axes. As shown in Fig. 2, the intensity distribution within the FOLZ discs included only two distinct excess lines with no evidence of other fine structure. The intensities of both lines varied between reflections and the inner line almost disappeared as the thickness was increased, being clear evidence of diffraction from Bloch states localized on strong atom strings. CBED patterns were acquired from thin crystals at 15 kV intervals over the range 100–250 kV. The

intensities of the inner FOLZ line for 70 independent reflections were measured on a six-point interval scale (0 to 5) by comparison with calibration lines, where reflections excited at two or more voltages were used to cross calibrate between negatives. As plotted in Fig. 3, the measured FOLZ reflections occupied a wide annulus between $20a^*$ and $28a^*$ with overall $3m$ symmetry. In a kinematic approximation, a unit change measured on the 0–5 intensity scale was equivalent to a resolution of 0.04 Å, or 10% of the planar spacing for a typical reflection. It was considered that more accurate measurement of the intensities was not justified, given that perturbations produced by coupling between FOLZ reflections could be quantified only by elaborate dynamical calculations based on a known structure. The intensities showed a clear hexagonal patterning confined to three lobes around the mirror lines, consistent with scattering centres located near the threefold screw axes at $\pm(1/3, 2/3)$ within the primitive projected cell [*cf*. Fig. 1(*b*)]. To avoid artifacts when calculating the Patterson transformation of Fig. 3, it was essential to use input data for the contouring routine based upon a fine mesh of grid points (200 × 200) within the projected cell to ensure adequate sampling of the short-wavelength components in the transform.

As a preliminary to discussion of the correlation peaks in $P^1(\mathbf{R})$, it is useful to derive the relevant space groups

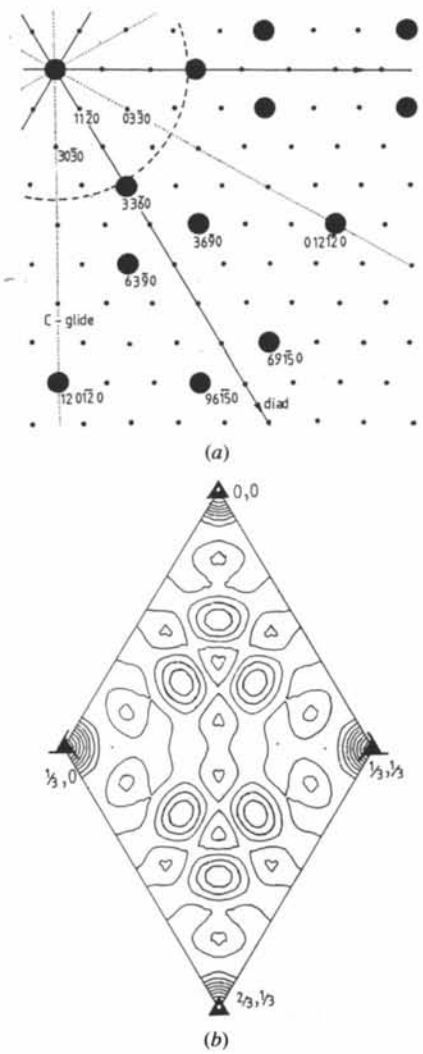

Fig. 1. (*a*) Schematic of *hki*0 reflections with high intensities relative to their neighbours, indexed from Kikuchi patterns. For comparison, the dashed circle represents the 2 Å resolution limit for a lattice image. (*b*) Fourier transform of (*a*) within a symmetry-reduced subcell, showing scattering centres around the $\bar{3}$ and $3_{1,2}$ axes.

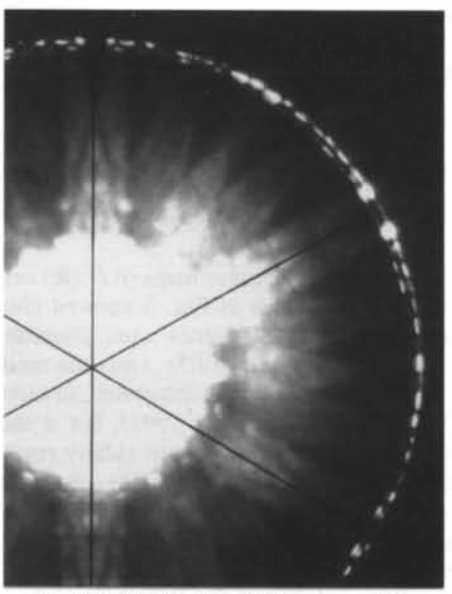

Fig. 2. Example of FOLZ reflections diffracted around the *c* axis of the *R* phase. The radial mirror lines are parallel to $\langle 10\bar{1}0 \rangle$ directions.

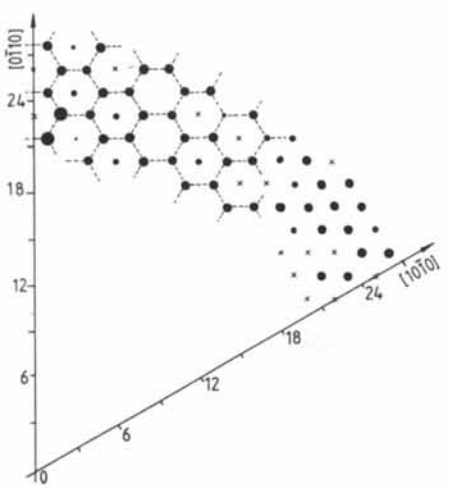

Fig. 3. Distribution of FOLZ intensites with $3m$ symmetry around the *c* axis of the *R* phase, measured from the inner excess line. The axes are indexed in multiples of a^*.

produced by conditional projection of the Patterson group $R\bar{3}m$ along the c axis. Generally, the space groups for conditional projections are isomorphic with the two-dimensional layer groups, listed in the Weber notation by Shubnikov & Koptsik (1974), where a symmetry operation across the layer plane is equivalent to a sign inversion. In the present example, the $\bar{3}$ axes through the vertices of the projected R cell are retained for the imaginary component of $P^1(\mathbf{R})$, but are transformed to sixfold rotation axes for the real component of $P^1(\mathbf{R})$. In the Weber notation, the corresponding layer groups are $p\bar{3}m1$ (no. 78) and $p6mm$ (no. 75) for the respective imaginary and real components. As sketched below, there are two formally equivalent routes between $U(\mathbf{r})$ and $P^n(\mathbf{R})$, but it is simpler in practice to derive the layer groups by projection of $P(\mathbf{r})$, rather than by auto-correlation of the complex function $U^n(\mathbf{R})$.

$$\begin{array}{ccc} U(\mathbf{r}) & \xrightarrow{\text{auto-correlation}} & P(\mathbf{r}) \\ \text{conditional projection} \downarrow & & \downarrow \text{conditional projection} \\ U^n(\mathbf{R}) & \xrightarrow{\text{auto-correlation}} & P^n(\mathbf{R}) \end{array}$$

The real and imaginary contour maps of $P^1(\mathbf{R})$ calculated from the FOLZ intensities in Fig. 3 showed clusters of three peaks close to the $3_{1,2}$ screw axes, consistent with atoms in the 18(e) positions of $R\bar{3}c$. Only the modulus of $P^1(\mathbf{R})$ is shown in Fig. 4, being illustrated, in more detail in Fig. 2 of Vincent & Exelby (1991), but it should be noted that the Patterson peaks were clearly resolved by the FOLZ reflections even though the projected atom centres were displaced by only 0.2 Å from the screw axes. However, background ripple in the transform due to series termination at the boundaries of the FOLZ annulus limited visibility of the Patterson peaks; in Fig. 4, only the three principal peaks around a screw axis were sufficiently defined for the interpretation by inspection of the contour map.

Following a detailed study of the literature, it became apparent that the Zn_4Sb_3 phase with the same space group and similar lattice parameters (Mayer, Mikhail & Schubert, 1978) was likely to be isostructural with the Al–Ge R phase. The coordination chemistry of Zn_4Sb_3 has not received much attention and therefore investigation of the R phase was continued, both to confirm the structure and also to establish the reliability of HOLZ Patterson transforms along suitable axes. For comparison, details of both structures are listed in Table 1, where Zn atoms in Zn_4Sb_3 occupy a set of general 36(f) positions, the 18(e) positions displaced by 0.27 Å from the screw axes are occupied by Zn and Sb atoms, and Sb atoms occupy 12(c) positions along the body diagonal of the primitive rhombohedral cell. A projection of the structure along the c axis (Fig. 5) was broadly consistent with the scattering centres visible in Fig. 1(b) around the threefold inversion and screw axes.

To confirm identification of the inner excess lines in FOLZ reflections with Bloch states localized on the 18(e) atoms, a many-beam dynamical program was used to calculate the dispersion, localization and excitation of Bloch states within the first Brillouin zone of the R phase projected along the c axis. The atomic parameters for Zn_4Sb_3 were used in the calculation with Al in the 36(f) positions and Ge in 12(c) and 18(e), equivalent to a composition of Al_6Ge_5. As expected, only three clusters of Bloch states showed significant excitation, where branch (1) was a strongly localized and weakly excited 1s state on the 12(c) atoms at the cell vertices, followed by branches (2) and (3) representing molecular combinations of 1s atomic Bloch states, which were centred on the screw axes and overlapped nearby Ge atoms in 18(e). The third branch cluster was a weakly bound set of 2s and 2p states with a large collective excitation that overlapped all Al and Ge strings. As mentioned above, the effective real-space potential for diffraction into a HOLZ reflection in layer n of the reciprocal lattice from Bloch state j is given by $\tau^{(j)}(\mathbf{R})U^n(\mathbf{R})$. For the Al_6Ge_5 structure, the Ge atoms in 12(c) are phased out of $U^n(\mathbf{R})$ for n odd because atoms are located at intervals $z, z+1/2$ along the c axis. It follows that the product

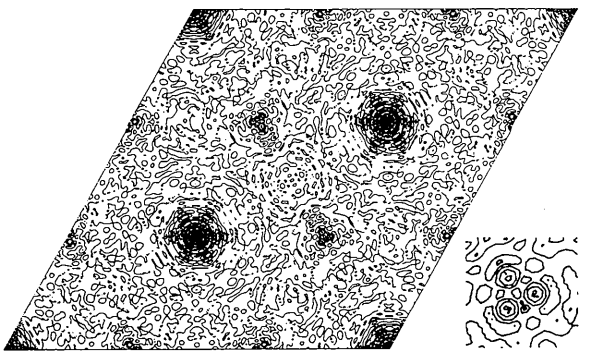

Fig. 4. Modulus of the Patterson transform calculated from the FOLZ intensities in Fig. 3. An example of the three correlation peaks clustered around the screw axes is enlarged on the lower right of the contour map.

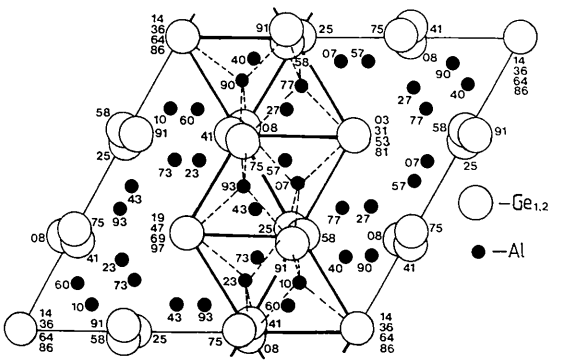

Fig. 5. Projection of the R-phase structure along the c axis, adapted from the Zn_4Sb_3 structure shown in Fig. 2 of Mayer *et al.* (1978). The outline of a single tetrahedral chain along $[10\bar{1}1]$ is shown. Fractional z coordinates are written as percentages.

$\tau^{(1)}(\mathbf{R})U^1(\mathbf{R})$ is almost zero, with no diffraction from branch (1) into FOLZ reflections. A similar absence of evidence for diffraction from branch (1) into reflections in the second HOLZ ring was explained by the predicted spacing of atoms in 12(c) at intervals close to $c/4$ (Table 1), implying that the string potential for 12(c) atoms remained weak for $U^2(\mathbf{R})$ and became stronger for $U^4(\mathbf{R})$. Unfortunately, Bragg diffraction into the fourth HOLZ ring was almost invisible relative to the diffuse background, giving no direct evidence for occupation of the 12(c) sites except the Fourier projection in Fig. 1(b).

The inner excess lines in FOLZ discs (Fig. 3) were identified with diffraction from branches (2) and (3) that fully overlapped the Ge atoms in 18(e). A similar geometry was considered by Bird (1985) for diffraction from zigzagged strings where $U^1(\mathbf{R})$ was represented by a two-dimensional Taylor expansion in the displacement parameter δ; it was shown that the Fourier coefficients of the product $\tau(\mathbf{R})U^1(\mathbf{R})$ were accurately proportional to the partial structure factors provided that δ was much smaller than the width of the overlapping Bloch state. A similar conclusion applies to the spiral strings considered here. Finally, the bright outer excess line in Fig. 2 was associated with diffraction from the cluster of 2s and 2p states with weak absorption and delocalized amplitudes. The calculated angular separation between the FOLZ excess lines was consistent with Fig. 1, thereby confirming the occupation of 18(e) sites by Ge; similar calculations with the locations of Al and Ge in the cell reversed showed smaller branch separation because the disparity in Al and Ge string strengths was reduced.

The utility of conditional Patterson transforms was further explored by calculations based on the intensities of outer excess lines in Fig. 1 but the transform showed no recognizable peaks. This result was not unexpected, given the large number of single-atom Al strings in the cell (Fig. 5) combined with the weak localization of the branch cluster throughout the cell. A similar exercise for FOLZ reflections around a $\langle 10\bar{1}1\rangle$ axis (parallel to a $\langle 100\rangle$ basis vector of the primitive cell) also produced no evidence for interpretable peaks in the contour map. Again, this failure was attributed to weak localization on the large number of single-atom strings in the projected cell, producing many weak peaks in the Patterson transform that were not visible above the series-termination ripple.

At this stage, the free parameter for the 18(e) atoms was refined by minimizing the r.m.s. difference between the observed intensities and calculations based on the geometric component of the structure factor for atoms in 18(e). It was decided to omit the atomic form factor and a Debye–Waller factor from the calculation because the experimental intensities showed no overall variation with scattering angle, which was attributed to the errors associated with the rescaling of FOLZ intensities recorded at different accelerating voltages. As discussed in the Appendix of Vincent *et al.* (1984), intensity differences were minimized in a standard least-squares refinement to provide a weighting factor towards stronger reflections, which were considered to be less susceptible to non-systematic dynamical perturbations. The refined value for the 18(e) position was 0.352 (1), equivalent to a displacement of 0.21 Å from the screw axes, with a separation of 0.35 Å between atom strings. The corresponding R factor [see equation (3)] for the mean difference between experimental and calculated amplitudes was 0.40, being comparatively large due to the absence of low-order reflections.

Table 2. *Comparison of observed and calculated X-ray powder intensities (I_o and I_c) for the R phase* (Cu $K\alpha$ *radiation*)

2θ (°)	d (Å)	$hkil$	I_o	I_c	$I_o - I_c$
15.49	5.717	$11\bar{2}1$	1	1	0
26.99	3.300	$30\bar{3}0$	100	100	–
27.74	3.213	$11\bar{2}3$	53	42	11
28.30	3.151	$12\bar{3}2$	20	20	0
31.98	2.796	$10\bar{1}4$	34	27	7
33.52	2.672	$13\bar{4}1$	17	15	2
35.72	2.412	$20\bar{2}4$	12	9	3
36.12	2.485	$13\bar{4}2$	2	3	−1
39.07	2.304	$22\bar{4}3$	38	40	−2
41.75	2.162	$14\bar{5}0$	3	4	−1
45.33	1.999	$13\bar{4}4$	30	23	17
47.67	1.906	$33\bar{6}0$	24	31	−7
48.14	1.889	$14\bar{5}3$	29	35	−6

4. X-ray powder diffraction data

To confirm the R-phase structure, X-ray powder patterns were acquired from crushed melt-spun Al–Ge ribbons that contained a mixture of the rhombohedral and monoclinic phases. Almost all of the peaks were indexed to either the R phase or to the monoclinic cell, where the lattice parameters of both phases were within 0.1% of the values listed by Kaufman & Fraser (1985). The peak intensities of 14 reflections from the R phase for 2θ between 15 and 50° are listed in Table 2 for comparison with intensities for the Al_6Ge_5 structure with Al in 36(f) and Ge in 18(e) and 12(c). X-ray structure factors were calculated for the Zn_4Sb_3 parameters and Debye–Waller factors (Mayer *et al.*, 1978), except for the 18(e) parameter refined from CBED patterns. Intensities were multiplied by the usual scaling factor to take account of polarization and the diffraction geometry, where

$$I \simeq [(1+\cos^2 2\theta)/(\sin^2\theta\cos\theta)]pF^2 \qquad (7)$$

and p is the multiplicity factor. When the calculated intensities were scaled to the most intense reflection, differences between I_o and I_c for the reflections in Table 2 averaged around 20%, which is clear evidence that the Zn_4Sb_3 and R phases were isostructural. The powder diffraction data were of sufficient quality that a Rietveld analysis to refine the structure would have been a practical option, although not attempted here.

5. The *R*-phase structure

A brief description of the *R* phase is given here, based on the parameters for Zn_4Sb_3 in Table 1 with Al in 36(*f*), Ge1 in 12(*c*) and Ge2 in 18(*e*). The structural unit is a tetrahedron of four Ge atoms (one Ge1 and three Ge2) that coordinates every Al atom. Unlike the equiatomic III–V and II–VI semiconductors where coordination tetrahedra share only vertices, Ge tetrahedra in the *R* phase share edges and form continuous linear chains along the $\langle 10\bar{1}1 \rangle$ directions parallel to the edges of the primitive rhombohedral cell (Fig. 5). Each tetrahedron is located within a single chain but shares vertices with other chains. Stability within chains is enhanced by anion bonds parallel to the *c* axis between pairs of Ge1 atoms; for $z = 0.137$ in 12(*c*) and $c = 11.66$ Å, the bond length is 2.64 Å. The Ge1 atoms are shared between three tetrahedra in separate chains, whereas the Ge2 atoms are shared between six tetrahedra divided equally between two chains. It follows that Ge1 is coordinated by three Al and one Ge, and Ge2 is coordinated by six Al atoms.

The polyanionic Al_6Ge_5 structure is consistent with a closed-shell configuration. If Ge1 receives 1 e (electron) from the anion bond and 3 e from the Al neighbours, the electron count is increased to eight on Ge1 and leaves 2 e on the Al atoms available for bonding to the three Ge2 neighbours. Therefore, each Ge2 receives 2/3 e from each Al, equivalent to 4 e from the six Al neighbours, increasing the electron count to eight for Ge2. This analysis is consistent with the rule for filled shells given by Pearson (1972), where

$$(n_a + n_c + b_a - b_c)/N_a = 8. \qquad (8)$$

n_a is the total number of valence-shell electrons from anions, n_c is the number contributed by cations, b_a is the number of anion bonds, n_c is the number of cation bonds and N_a is the number of anions. For $n_a = 5 \times 4$, $n_c = 6 \times 3$, $b_a = 2$, $b_c = 0$ and $N_a = 5$, we have $(20 + 18 + 2 - 0)/5 = 8$, implying that the *R* phase with ideal stoichiometry may be a semiconductor. The equiatomic composition measured from EDX spectra was not entirely consistent with the ideal formula Al_6Ge_5, but some small disparity was not unexpected, given the likelihood of mixed site occupancies in a rapidly quenched structure.

6. Discussion

The problem of *ab initio* structure determination by electron diffraction has no simple solution except for crystals where the kinematic approximation is applicable to the majority of reflections. For crystals that contain heavier atoms, dynamical diffraction within the net of zero-layer reflections around a major axis is unavoidable and therefore the structural analysis of a metastable Al–Ge phase was attempted using principally the intensities of HOLZ reflections. The channelling of the incident beam into Bloch states localized on symmetry-related subsets of atom strings was turned to advantage because the amplitudes of associated HOLZ excess lines were proportional to the partial structure factors for these atoms. The corresponding Patterson transform was restricted to summation over an annulus of high-order reflections and showed sharp correlation peaks that were directly interpretable and allowed the positions of a subset of atoms to be refined. A further advantage might be obtained by applying maximum-entropy techniques to reduce ripple in the transform and improve the visibility of correlation peaks relative to the background.

However, HOLZ Patterson transforms lack generality in that we require a zone axis where a subset of atoms project into strong well separated strings with positions defined by at least one free parameter. Most projections are likely to prove unsuitable; even for favourable zone axes, the weaker string potentials are not associated with localized Bloch states and are not expected to be visible above the background ripple in HOLZ transforms. This view may be unduly pessimistic, in that even partial information about an unknown structure is sufficient to encourage an educated guess that may be confirmed either by simulation of dynamical CBED patterns or by comparison with X-ray powder patterns. The latter route was followed for the *R* phase, where the agreement between observed and calculated powder intensities confirmed the structure. It is considered that the combination of CBED analysis to determine the space group and some atomic parameters with modern X-ray powder techniques represents the most efficient method for structure determination for mixtures of sub-micrometre crystals.

One of us (DRE) acknowledges financial support from the Science and Engineering Research Council.

References

BIRD, D. M. (1985). *J. Phys. C*, **18**, 481–498.

BIRD, D. M. (1989). *J. Electron Microsc. Tech.* **13**, 77–97.

BIRD, D. M. & SAUNDERS, M. (1992). *Acta Cryst.* A**48**, 555–562.

COENE, W., JANSSEN, G., OP DE BEECK, M. & VAN DYCK, D. (1992). *Phys. Rev. Lett.* **69**, 3743–3746.

COWLEY, J. M. (1965). *Prog. Mater. Sci.* **13**, 267–321.

DONG, W. BAIRD, T., FRYER, J. R., GILMORE, C. J., MACNICOL, D. D., BRICOGNE, G., SMITH, D. T., O'KEEFE, M. A. & HÖVMOLLER, S. (1992). *Nature (London)*, **355**, 605–609.

DORSET, D. L. (1991). *Ultramicroscopy*, **38**, 23–40.

DORSET, D. L. (1992). *Ultramicroscopy*, **45**, 5–14.

KAUFMAN, M. J. & FRASER, H. L. (1985). *Acta Metall.* **33**, 191–203.

LICHTE, H. (1992). *Ultramicroscopy*, **47**, 223–230.

MA, Y., ROMMING, C., LEBECH, B., GJØNNES, J. & TAFTØ, J. (1992). *Acta Cryst.* B**48**, 11–16.

MAYER, H. W., MIKHAIL, I. & SCHUBERT, K. (1978). *J. Less Common Met.* **59**, 43–52.

PEARSON, W. B. (1972). *The Crystal Chemistry and Physics of Metals and Alloys*. New York: Wiley-Interscience.

SHUBNIKOV, A. V. & KOPTSIK, V. A. (1974). *Symmetry in Science and Art*. New York: Plenum Press.

SPENCE, J. C. H. & ZUO, J. M. (1992). *Electron Microdiffraction*. New York: Plenum Press.

VAINSHTEIN, B. K., ZVYAGIN, B. B. & AVILOV, A. S. (1992). *Electron Diffraction Techniques*, Vol. 1, edited by J. M. COWLEY, pp. 216–312. IUCr/Oxford Univ. Press.

VINCENT, R. & BIRD, D. M. (1986). *Philos. Mag.* **A53**, L35–L40.

VINCENT, R. BIRD, D. M. & STEEDS, J. W. (1984). *Philos. Mag.* **A50**, 765–786.

VINCENT, R. & EXELBY, D. R. (1991). *Philos. Mag. Lett.* **63**, 31–38.

VINCENT, R. & EXELBY, D. R. (1993). *Philos. Mag.* **B68**, 513–528.

VINCENT, R. & WITHERS, R. L. (1987). *Philos. Mag. Lett.* **56**, 57–62.